KAMPALA INTERNATIONAL UNIVERSITY

KIU
Journal of Science, Engineering and Technology

KJSET Research Article

Design and finite element validation of a spring-assisted flywheel energy storage system for groundwater pumping in rural Uganda

Kabagambe Edward[1,2], Dr. Samuel George Onep [1], Associate Prof. P. Sathish Kumar [1]

Department of Mechanical Engineering, Kampala International University, Uganda

Department of Mechanical Engineering, Kabale University, Uganda[4]

edward.kabagambe@studwc.kiu.ac.ug[1], ekabagameb@kab.ac.ug[2], sathishpauto@kiu.ac.ug[1], onep.samuel@kiu.ac.ug[1]

Corresponding Author: edward.kabagambe@studwc.kiu.ac.ug

Paper history:

Received 11 March 2026

Accepted in revised form 20 May 2026

Keywords

Low-speed flywheel; Torsion spring assist; Off-grid water supply; Structural validation; Fatigue life prediction; Appropriate technology; Rural energy access

Abstract

Off-grid rural communities in Uganda lack reliable energy for groundwater pumping, with existing solutions constrained by high costs, limited lifespans, and environmental concerns. This paper presents the design and finite element validation of a spring-assisted flywheel energy storage system (FESS) developed for this context. The system was modeled in SolidWorks 2025 and analyzed using Ansys 2025 R2 STUDENT, incorporating a 50 kg mild steel flywheel (6.25 kg·m² moment of inertia), a spring-assist mechanism comprising two sets of three torsion springs (18.5 Nm/rad stiffness per spring, configured to deliver 35 Nm supplemental torque at the flywheel shaft when fully deflected to 120°), and a 2:1 belt-pulley drive. Static structural analysis confirmed exceptional structural integrity: the shaft exhibited maximum principal stress of 0.294 MPa (0.05% of yield strength) with factor of safety of 15, while the frame showed maximum deformation of 0.78 mm, von Mises stress of 18.5 MPa, and factor of safety of 13.5, substantially exceeding the recommended minimum of 3.0. Modal analysis identified critical speeds at 6,760 RPM, 9,762 RPM, and 17,593 RPM, establishing three resonance-free operating windows: below 5,700 RPM; 7,800–9,500 RPM; and 11,300–14,900 RPM. Based on human arm cranking literature, manual operation is expected to achieve only 95–267 RPM, well within the lowest and safest window (<5,700 RPM). The higher windows represent absolute structural limits, not operational targets. The validated design provides a technically sound foundation for prototype fabrication, offering a battery-free, mechanically robust alternative aligned with Uganda's rural energy needs and Sustainable Development Goals for clean water and energy access.

Acronyms

Acronym	Full Form
ASTM	American Society for Testing and Materials
AISI	American Iron and Steel Institute
CAD	Computer-Aided Design
FEA	Finite Element Analysis
FESS	Flywheel Energy Storage System
FOS	Factor of Safety
ISO	International Organization for Standardization
RPM	Revolutions Per Minute
SDG	Sustainable Development Goals
UBOS	Uganda Bureau of Statistics
UN	United Nations

1.0 Introduction

The interconnected challenge of ensuring reliable access to energy and water remains a persistent global issue, fundamental to achieving the Sustainable Development Goals [1]. In off-grid communities worldwide, groundwater pumping is constrained by the availability of sustainable power. Solar energy has emerged as a leading alternative, but its natural intermittency requires robust energy storage, a role traditionally filled by electrochemical batteries. These are often limited by high lifecycle costs, limited operational lifespans, and complex environmental disposal problems, driving the global search for more durable alternatives [2]. Similarly, diesel-powered generators, while common, introduce prohibitive fuel costs and substantial greenhouse gas emissions [3].

This challenge is particularly severe in Sub-Saharan Africa, which bears the world's highest burden of energy poverty [4]. The region depends heavily on groundwater, yet the transition to mechanized pumping is constrained by the limitations of existing energy systems. While solar pumping has been widely promoted, its dependency on battery-based storage has led to system failures and unsustainable maintenance costs, thus undermining long-term water security across the continent [5].

Uganda exemplifies this regional crisis. Over 90% of the rural population lacks access to electricity, and even grid-connected regions experience frequent outages [6, 7]. Groundwater is a vital source in rural Uganda, especially where piped infrastructure is scarce. Many rural communities rely on manually operated boreholes and springs, which are physically demanding and unsustainable, particularly during dry spells [8]. Diesel-powered pumps, though widely used, are increasingly unsustainable due to high fuel costs, and accessibility challenges by smallholder farmers which increases their vulnerability to market fluctuations of fuel, that further reduces their income [3]. Solar-powered systems, though cleaner, depend on consistent irradiance, and their reliability diminishes during Uganda's frequent cloudy and rainy seasons, necessitating battery storage with its attendant limitations [2, 6].

Flywheel Energy Storage Systems (FESS) present a promising mechanical alternative, offering virtually unlimited cycle life, rapid charge-discharge rates, zero operational emissions, and potential for local fabrication using readily available materials [9]. Using a solid steel flywheel with a spring-assist mechanism, such a system can sustain pump operations during cloudy periods without the need for chemical storage. However, FESS remains underutilized in Uganda due to design complexity, lack of adaptation for local fabrication, and insufficient empirical research on their application for rural water pumping [10].

This study addresses this gap by presenting the design and finite element validation of a spring-assisted FESS specifically developed for groundwater pumping in rural Uganda. The system incorporates a novel spring-assist mechanism to sustain flywheel rotation, mitigating the inherent challenge of intermittent manual input. The design prioritizes locally available materials, structural integrity, and safety, ensuring contextual feasibility alongside technical performance.

2.0 Design Methodology

2.1 System Design Specifications

The system was designed to meet context-specific requirements for rural Uganda: a target pumping head of 10 meters, flow rate of 5–10 liters per minute, and minimum operational duration of 5 minutes after manual charging [7, 8]. Based on published data on human arm cranking performance [13], the anticipated rotational speed range for manual operation is 95–267 RPM. Table 1 presents the finalized engineering specifications.

Table 1: Final component sizing and design parameters

Component	Parameter	Value	Unit	Justification
Flywheel	Outer Diameter	1000	mm	Selected to achieve target moment of inertia (6.25 kg·m²) using $I = ½mr^2$ [16]; provides energy density of 49 J/kg at expected max human speed (267 RPM) [13]
	Thickness	100	mm	Provides adequate mass for energy storage
	Mass	50	kg	Calculated from volume and density (7850 kg/m³)
	Material	ASTM A36 Mild Steel	-	High density, machinability, local availability
	Moment of Inertia (I)	6.25	kg·m²	Calculated for solid disk of 50 kg using $I = ½mr^2$
Shaft	Diameter	100	mm	Sized to withstand flywheel weight and stresses

	Material	AISI 1045 Medium Carbon Steel	-	Yield strength 530 MPa, machinable
Spring-Assist	Torsional Stiffness (k)	18.5	Nm/rad	Provides 35 Nm supplemental torque at 120° deflection
	Maximum Angular Deflection	120	°	Limited by spatial constraints and material elasticity
Belt-Pulley	Flywheel Pulley Diameter	500	mm	Provides 2:1 speed increase
	Alternator Pulley Diameter	250	mm	
	Speed Ratio	2:1	-	Ensures alternator reaches operational speed
Bearings	Type	Sealed Deep Groove Ball	-	100 mm bore, sealed for contaminant protection
Frame	Material	Mild Steel Square Hollow Section	-	120×80×5 mm, locally available

2.2 Analytical Foundation

The kinetic energy stored in the flywheel is governed by the fundamental relationship for rotational kinetic energy;

$$E = \frac{I\omega^2}{2} \qquad (1)$$

For the selected solid disk geometry, the moment of inertia was calculated as;

$$I = \frac{1}{2}mr^2 \qquad (2)$$

$$Inertia, I = \frac{1}{2} \times 50 \times 0.5^2 = 6.25\ kgm^2$$

The spring-assist mechanism was modeled using Hooke's Law for rotational systems. The restorative torque exerted by the torsion spring is;

$$T_s = k\theta \qquad (3)$$

The required stiffness to deliver a target supplemental torque of 35 Nm at 120° deflection (2.09 rad) was calculated as;

$$\text{Stiffness, } k = \frac{T_s}{\theta} = \frac{35\ \text{Nm}}{2.09\ \text{rad}} = 16.7\text{Nm/rad}$$

A final stiffness of 18.5 Nm/rad was specified, incorporating a 10% design margin. The elastic potential energy stored at full deflection is;

$$E_s = \frac{1}{2}k\theta^2 \qquad (4)$$

$$Elastic\ potential\ energy, E_s = \frac{1}{2} \times 18.5\ \times 2.09^2 = 40.404\ J$$

The belt-pulley speed ratio was determined solely by the selected pulley diameters;

$$R_{BP} = \frac{\text{alternator rpm}}{\text{Flywheel rpm}} = \frac{D_a}{D_f} \qquad (5)$$

Where R_{BP} = Belt − Pulley ratio, D_a = diameter of alternator pulley and D_f = diameter of flywheel pulley

$$Speed\ Ratio = \frac{500}{250} = 2:1$$

2.3 Spring Mechanism Operation

The spring-assist mechanism consists of two opposing sets of torsion springs mounted on the flywheel shaft. At rest, both spring sets are in a neutral, balanced position, neither wound nor unwound.

During manual charging, rotation of the hand crank causes one spring set to wind (storing elastic potential energy) while the opposing set unwinds (releasing energy). Because the two sets oppose each other, the net resistive torque experienced by the user is only the difference between the wound and unwound spring forces, which remains negligible throughout the cranking motion. The springs therefore do not resist manual input.

After manual input ceases, the alternating wound-unwound cycle continues, with the springs applying a supplemental torque directly to the flywheel shaft. This torque counteracts deceleration from bearing friction and pump load, sustaining rotation and extending operational duration. The spring parameters (k = 18.5 Nm/rad per spring, maximum deflection 120°) were selected to deliver approximately 35 Nm supplemental torque at full deflection, sufficient to meaningfully extend runtime based on estimated system losses [11] while remaining within human capability limits [13].

2.4 Computer-Aided Design

The engineering specifications were translated into a comprehensive three-dimensional virtual prototype using SolidWorks 2025. Figure 1 shows the complete system assembly, illustrating the integration of the flywheel, double-torsion spring mechanism, structural frame, and alternator.

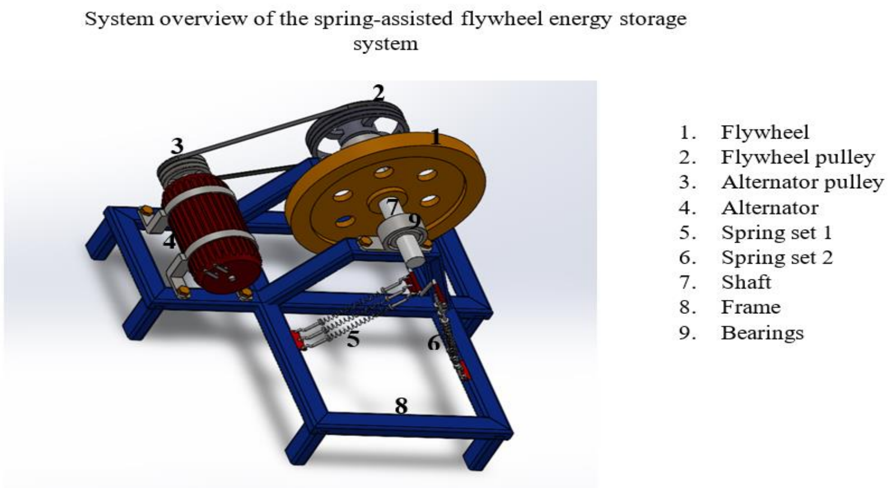

Figure 1: Complete system overview of the spring-assisted flywheel energy storage system modeled in SolidWorks 2025.

The virtual assembly verified geometric compatibility, confirmed proper clearances between moving and stationary parts, and ensured correct belt alignment. Mass properties calculated from the CAD model showed close agreement with analytical values (modeled flywheel mass 47.60 kg, 4.8% below design target; moment of inertia 7.29 kg·m², 16.6% higher due to three-dimensional geometry effects).

2.5 Finite Element Analysis Setup

Finite element analysis was conducted using Ansys 2025 R2 STUDENT to validate structural integrity. Two distinct analyses were performed: static structural analysis on the shaft and frame, and modal analysis on the flywheel. Material properties were assigned per design specifications (Table 2).

Table 2: Material properties assigned in FEA

Component	Material	Yield Strength (MPa)	Elastic Modulus (GPa)	Poisson's Ratio
Shaft	AISI 1045	530	205	0.29
Frame	Mild Steel	250	200	0.30
Flywheel	ASTM A36	250	200	0.30

2.5.1 Boundary Conditions

For the shaft, a remote force of 490 N was applied to simulate the gravitational load of the 50 kg flywheel. Fixed supports were applied at bearing locations, representing the restraint imposed by bearing housings.

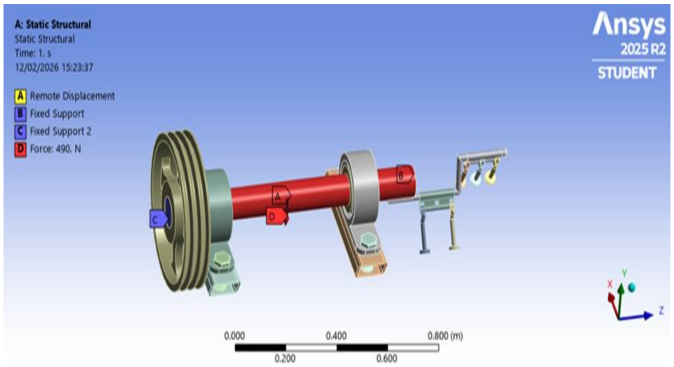

Figure 2: Boundary conditions applied to shaft showing fixed supports at bearing locations and applied force of 490 N representing 50 kg flywheel weight.

For the frame, a total downward load of 686 N was applied to bearing support pedestals, accounting for combined weight of flywheel (490 N), shaft (78.45 N), pulleys (78.45 N), and bearings (58.84 N). Fixed constraints were applied at the six base stands.

For modal analysis, the flywheel was modeled with deformable body behavior. Displacements in X, Y, and Z directions were constrained to zero, rotations about X and Y axes fixed, while rotation about the Z axis was permitted free, accurately representing operational freedom.

2.5.2 Meshing and Simulation Parameters

The shaft was meshed with 67,200 nodes (26,363 elements), the frame with 47,421 nodes (12,725 elements), and the flywheel (modal analysis) with 26,746 nodes (15,260 elements). Tetrahedral elements with local refinement at stress concentrations (bearing seats, keyways, spring attachments) were used; element sizes: shaft ~3 mm, frame ~5 mm, flywheel ~10 mm. Average aspect ratio <5, skewness <0.85. A mesh convergence study refined the element size until the change in maximum von Mises stress between successive refinements fell below 5%, which the final meshes satisfied.

All materials were modelled as linear elastic and isotropic, except the spring (AISI 6150) which used bilinear isotropic hardening (tangent modulus = 1% of elastic modulus). Perfect bonding was assumed at contacts. Static structural loads: remote forces (490 N shaft, 686 N frame) with fixed supports at bearings; spring torque applied as a 35 Nm moment; gravity (9.81 m/s²) included. Modal analysis considered only rotational inertia. Solver: Ansys 2025 R2 STUDENT, static structural with large deflection off, direct sparse solver, force residual <0.001. Modal analysis used Block Lanczos eigensolver (6 modes).

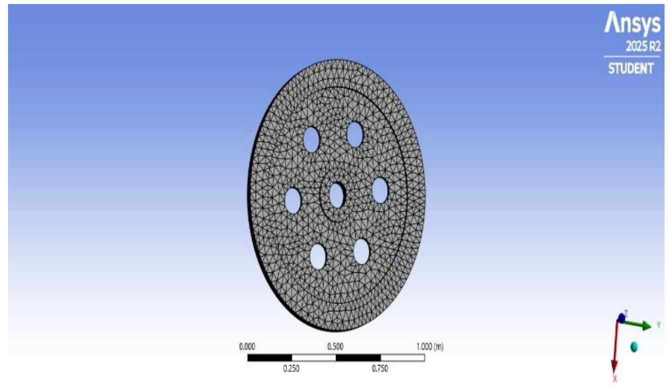

Figure 3: Finite element mesh of flywheel assembly generated in Ansys 2025 R2 STUDENT.

3.0 Results and Discussion

3.1 Static Structural Analysis

Static structural analysis was performed to evaluate stress distribution and total deformation in the two-primary load-bearing components, the shaft and the support frame, under peak design loads.

3.1.1 Shaft Analysis

Figure 4 presents the maximum principal stress distribution in the shaft under the applied 490 N load.

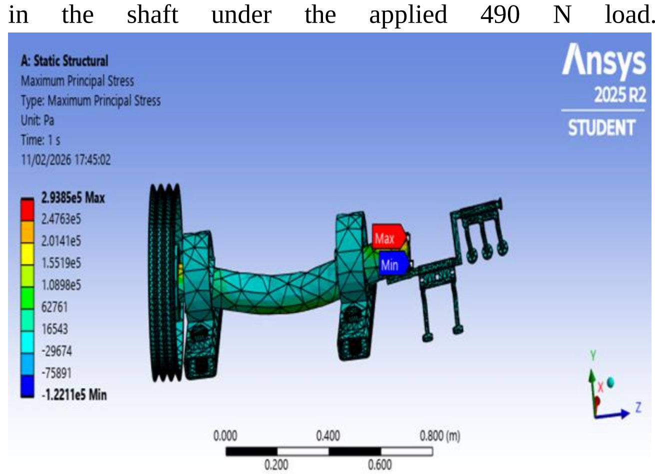

Figure 4: Maximum principal stress distribution in the shaft under a 490 N flywheel load. The peak stress of 0.294 MPa occurs at the bearing contact region, which is only 0.05% of the material's yield strength (530 MPa). This indicates an extremely safe design with negligible risk of brittle fracture.

The maximum principal stress of 0.294 MPa is exceptionally low, merely 0.05% of the material's yield strength (530 MPa). This confirms that the shaft operates well within the elastic regime with negligible risk of brittle fracture or fatigue failure. The negative principal stresses (compressive) observed in some regions indicate portions of the shaft are in compression, which is favorable as materials are generally stronger in compression than tension.

Figure 5 shows the total deformation of the shaft.

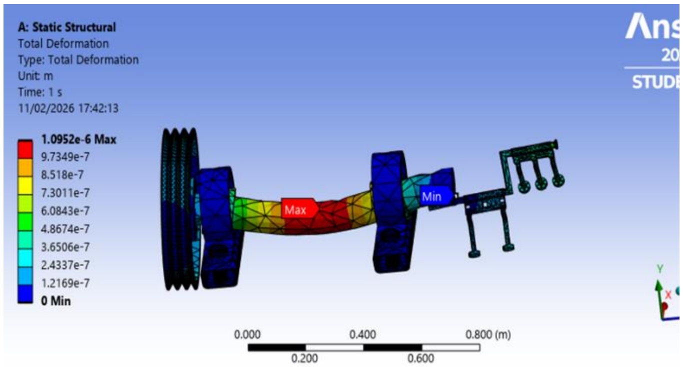

Figure 5: Total deformation of the shaft. The maximum displacement of 1.0952 × 10⁻⁶ m (≈1.1 μm) occurs at the mid-span where the flywheel is mounted. This sub-micron deflection ensures that belt alignment and bearing clearances are maintained."

The maximum deformation of 1.0952×10^{-6} m (approximately 1.1 micrometres) is equivalent to roughly one-hundredth the diameter of a human hair. This exceptional stiffness ensures that critical alignments between shaft, bearings, and belt drive system are maintained during operation, preserving transmission efficiency and preventing premature component wear.

Figure 6 presents the factor of safety distribution.

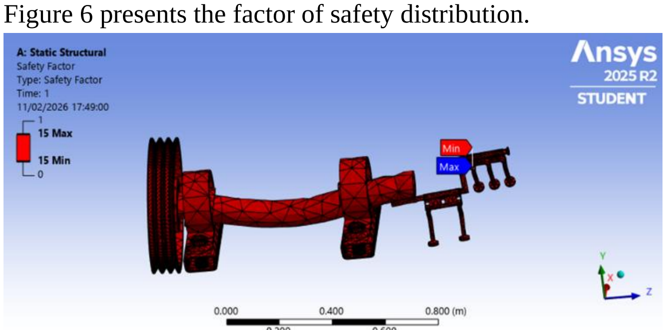

Figure 6: Factor of safety distribution for the shaft. The minimum FOS is 15, far exceeding the recommended minimum of 3.0. This large safety margin accommodates unexpected overloads and shock loads.

The minimum factor of safety of 15 significantly exceeds the recommended minimum of 3.0 for rotating machinery applications [9]. This substantial safety margin indicates the shaft can withstand unexpected overloads, shock loads during manual cranking, and potential stress concentrations without risk of failure.

Design robustness considerations

While the factors of safety (15 and 13.5) substantially exceed typical engineering requirements, this level of robustness is intentional for the rural Ugandan context. The system must withstand not only designed loads but also unexpected dynamic forces, including children potentially climbing on or sitting on the stationary flywheel, a realistic scenario in community settings where unsupervised access may occur. The minimal deformation (shaft: 1.1 μm; frame: 0.78 mm) confirms that the selected materials (ASTM A36, AISI 1045) are well-suited for the application, providing stiffness that ensures long-term alignment and reliability. Additionally, these high safety margins create opportunities for future adaptations, such as motorized drive systems, without requiring complete redesign. While material optimization could reduce costs, the current design prioritizes safety, durability, and contextual robustness over marginal material savings. Future iterations may explore optimized geometries as suggested in Section 6.0, balancing cost reduction with maintained safety.

3.1.2 Frame Analysis

Figure 7 shows the total deformation of the support frame under the combined 686 N load.

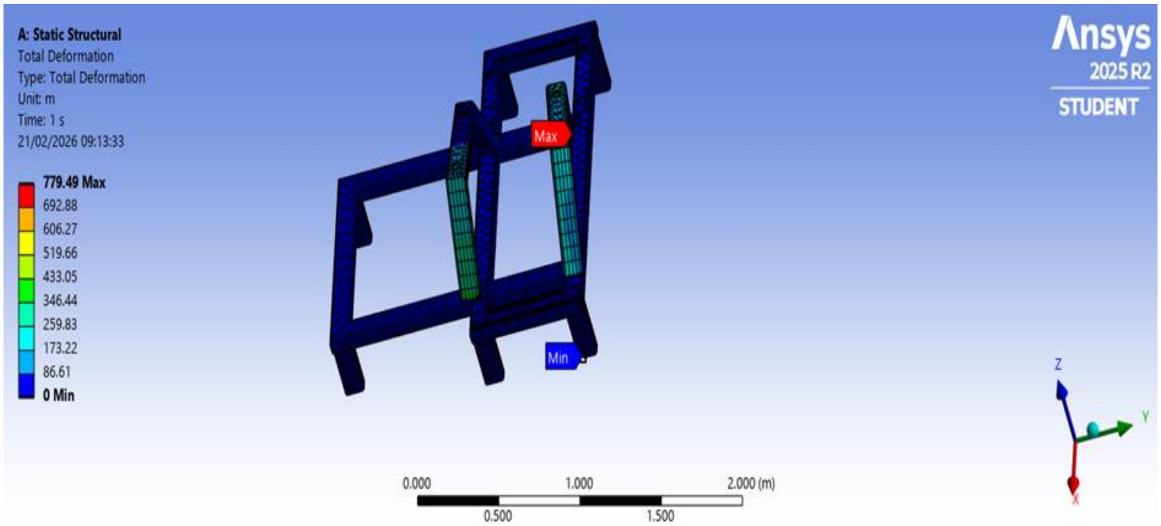

Figure 7: Total deformation of support frame showing maximum displacement of 0.78 mm at top center where heaviest components are mounted.

The maximum deformation of 0.779 mm is minimal relative to overall frame dimensions. This level of stiffness ensures component alignment is maintained, dynamic instability is avoided, and structural integrity remains uncompromised during manual operation.

Figure 8 presents the equivalent von Mises stress distribution.

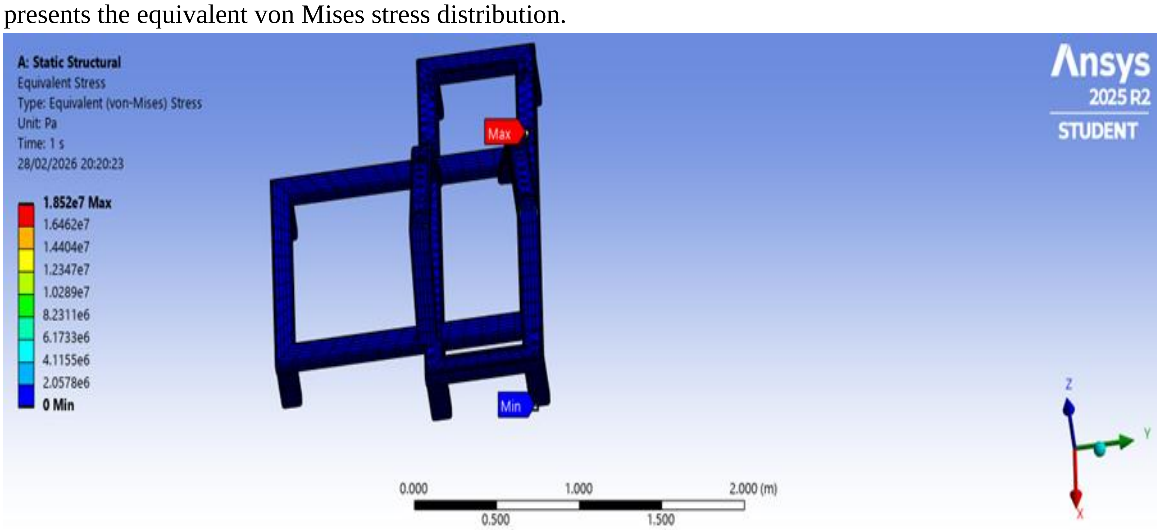

Figure 8: Equivalent von Mises stress in the frame. The maximum stress of 18.5 MPa occurs at the joint locations, representing only 7.4% of the material's yield strength (250 MPa).

Figure 9 shows the factor of safety distribution for the frame.

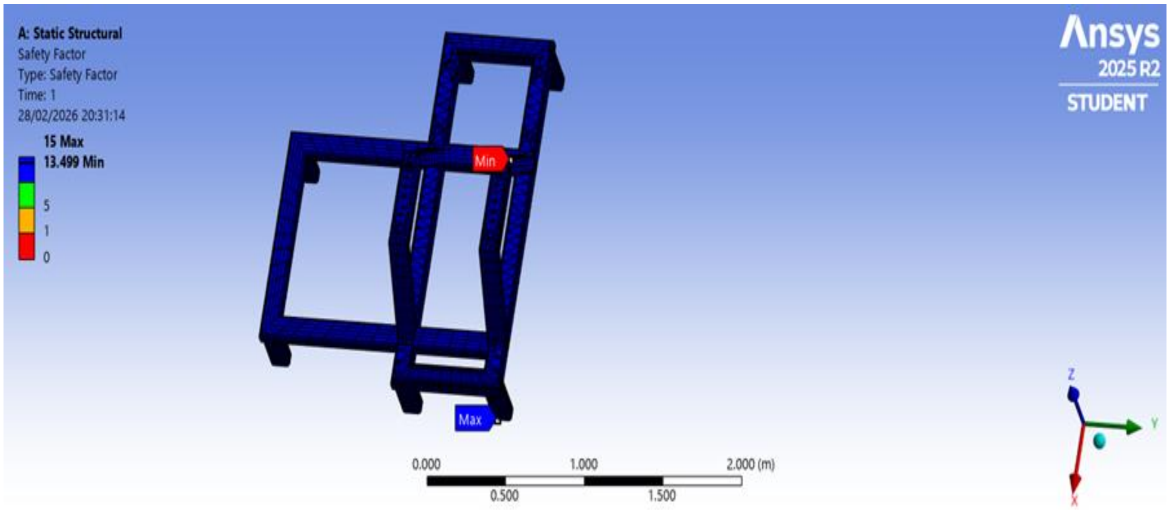

Figure 9: Factor of safety distribution for the frame. The minimum FOS is 13.5 at the critical joints, providing a very conservative design.

The minimum factor of safety of 13.5 at critical joints, more than four times the recommended minimum of 3.0, means the frame can withstand loads nearly fourteen times greater than the applied 686 N before yielding would occur. This provides confidence that the structure will withstand not only static loads but also dynamic forces and vibrations during manual operation.

Summary of static structural analysis results

The shaft exhibited a maximum principal stress of 0.294 MPa, representing merely 0.05% of its yield strength, with a maximum deformation of 1.1×10^{-6} m and a minimum factor of safety of 15. The frame showed a maximum von Mises stress of 18.5 MPa, equivalent to 7.4% of its yield strength, with a maximum deformation of 0.78 mm and a minimum factor of safety of 13.5. Both components substantially exceed the recommended minimum factor of safety of 3.0 for rotating machinery.

3.2 Modal Analysis

Modal analysis was performed to determine natural frequencies and corresponding mode shapes of the flywheel, important for identifying rotational speeds that must be avoided to prevent resonant amplification of vibrations. Table 3 presents the first six natural frequencies extracted from the analysis.

Table 3:Natural frequencies extracted from modal analysis

Mode	Frequency (Hz)	Mode Shape Description
1	7.7836×10^{-4}	Rigid body rotation (Z-axis)
2	112.64	First tilting mode
3	112.69	Orthogonal tilting mode
4	162.70	Higher-order bending
5	293.21	Complex rim wave pattern
6	293.22	Orthogonal rim wave pattern

Mode 1 at 0.000778 Hz represents rigid body rotation about the Z-axis, confirming boundary conditions were correctly implemented with rotational freedom. This mode involves no structural deformation and poses no risk to flywheel integrity. Modes 2 and 3 form a closely-spaced pair at approximately 112.6 Hz, representing orthogonal tilting behaviors.

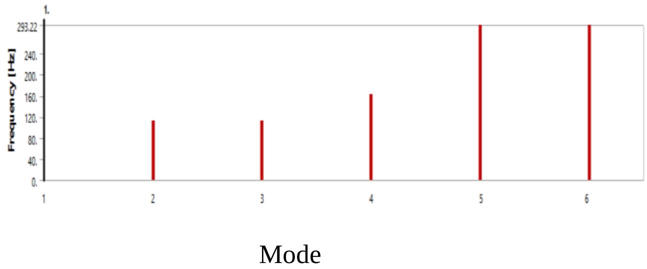

Figure 10: Graphical representation of the first six modes against natural frequencies generated by Ansys 2025 R2 Student.

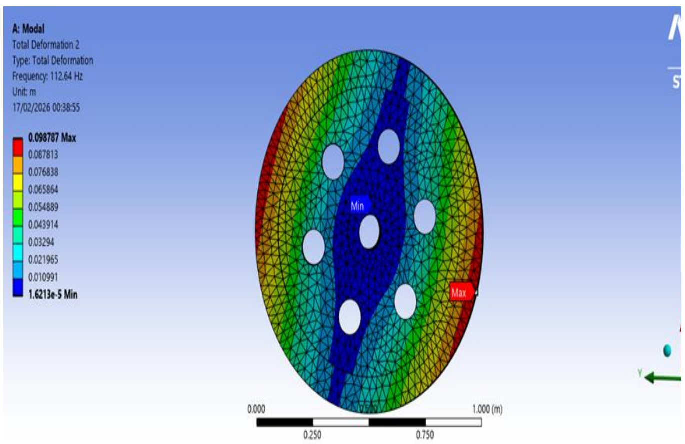

Figure 11: Mode 2 shape at 112.64 Hz. The maximum displacement of 0.0988 m occurs at the rim. This tilting mode would generate significant dynamic stresses if excited, but the operating speed is far below this frequency.

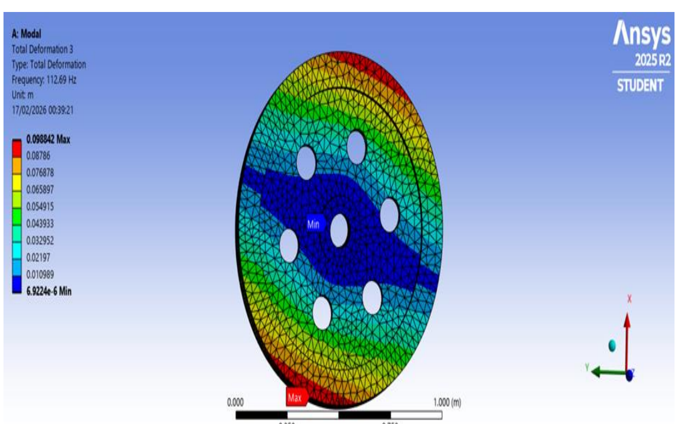

Figure 12: Mode 3 shape at 112.69 Hz, showing the orthogonal tilting pattern perpendicular to Mode 2 with nearly identical frequency and deformation magnitude produced in Ansys 2025 R2 Student.

These modes exhibit the largest deformation amplitudes among structural modes (0.0988 m maximum), indicating that significant dynamic stresses could be generated if excited.

Mode 4 at 162.70 Hz exhibits more complex bending with reduced deformation amplitude (0.0666 m), suggesting greater structural stiffness at this higher frequency.

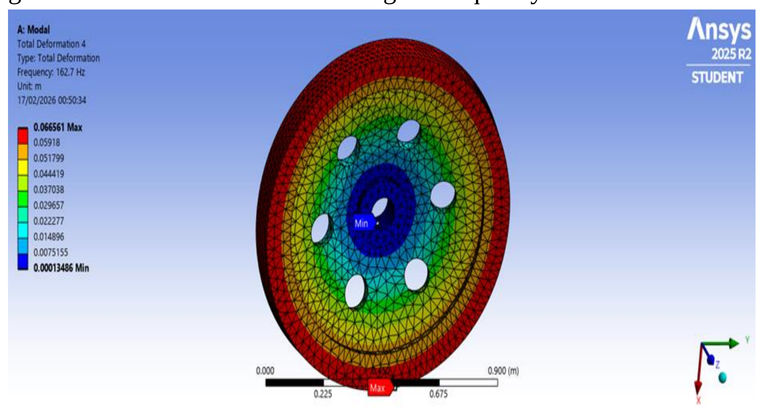

Figure 13: Mode 4 shape at 162.70 Hz, showing higher-order bending with reduced maximum deformation of 0.0666 meters compared to lower modes generated in Ansys 2025 R2 Student.

Modes 5 and 6 form another paired set at approximately 293.2 Hz, representing complex circumferential rim wave patterns.

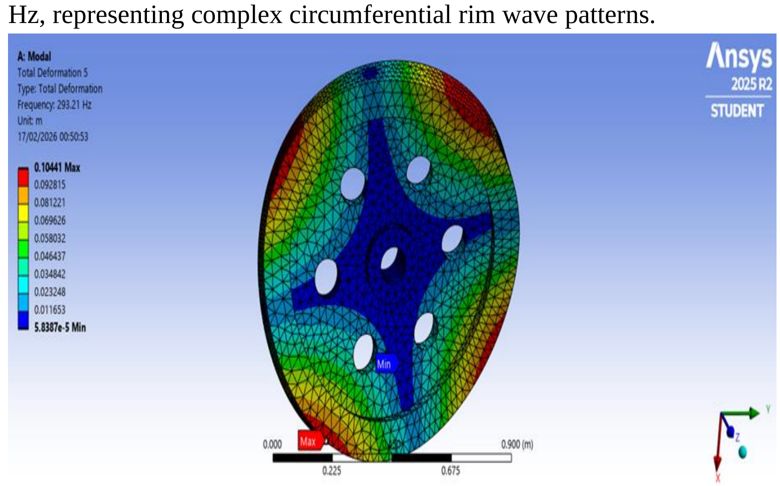

Figure 14: Mode 5 shape at 293.21 Hz, showing complex circumferential wave pattern with maximum deformation of 0.1044 meters at the rim generated in Ansys 2025 R2 Student

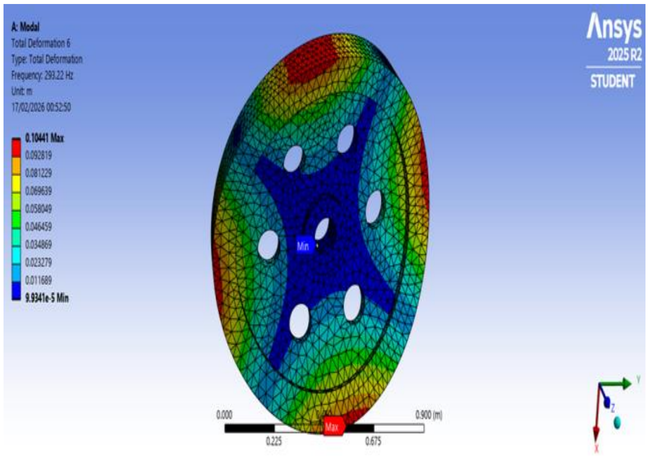

Figure 15:Mode 6 shape at 293.22 Hz, showing the orthogonal rim wave pattern paired with Mode 5 at nearly identical frequency and deformation magnitude produced in Ansys 2025 R2 Student.

Modes 2 and 3 form a closely-spaced pair at approximately 112.6 Hz, representing orthogonal tilting behaviors with maximum deformation of 0.0988 m. Mode 4 at 162.70 Hz exhibits more complex bending with reduced deformation amplitude (0.0666 m). Modes 5 and 6, however, show the highest deformation amplitudes of 0.1044 m, representing complex circumferential rim wave patterns that would generate severe cyclic stresses if excited.

Critical speeds were calculated from natural frequencies using equation 6.

$$RPM = Frequency\ (Hz) \times 60 \qquad (6)$$

Table 4: Critical speeds and recommended avoid ranges

Modes	Natural Frequency (Hz)	Critical Speed (RPM)	Avoid Range (±15%)	Operating Recommendation
2 & 3	*112.64 / 112.69*	*6,758 / 6,761*	*5,744 – 7,772 RPM*	***Primary safe window*** *Below 5,700 RPM*
4	*162.70*	*9,762*	*8,298 – 11,226 RPM*	***Not recommended*** *- Documented for completeness only* *7,800 – 9,500 RPM*
5 & 6	*293.21 / 293.22*	*17,593 / 17,593*	*14,954 – 20,232 RPM*	***Unsafe for sustained operation*** *- High deformation risk* *11,300 – 14,900 RPM*

Applying a conservative 15% safety margin around each critical speed yields the following guidance:

1. **Low-speed window (Below 5,700 RPM)**

This is the only recommended operating regime for sustained use. It avoids all resonance zones completely, operates below the first critical speed, and provides maximum safety margin. None of the mode shapes are excited in this region.

2. **Mid-speed window (7,800–9,500 RPM)**

While technically resonance-free, this window lies between modes with significant deformation amplitudes (0.0988 m). Operation in this region is not recommended for the manually-powered system, as inadvertent excitation of nearby modes could generate substantial vibrations.

3. **High-speed window (11,300–14,900 RPM)**

This window should be avoided entirely for sustained operation. Modes 5 and 6, with deformation amplitudes of 0.1044 m, pose unacceptable risks of fatigue-inducing cyclic stresses and potential structural damage if excited. This window is documented only to establish absolute structural limits and should not be considered an operational target.

It must be emphasized that the critical speeds identified here represent absolute structural limits, not operational targets. Based on human power capability [13], manual operation is expected to achieve only 95–267 RPM, well within the only recommended operating regime (below 5,700 RPM). The higher windows are documented for completeness and to guide future adaptations should alternative power sources be developed, but they come with significant vibrational risks that would require additional analysis and mitigation.

3.3 Expected Human-Powered Performance in Context

To contextualize these structural limits within real-world operation, published data on human arm cranking performance was consulted. Vanderthommen et al. [13] measured peak angular velocities during maximal arm cranking exercise in healthy subjects, reporting values of 13–28 rad/s (124–267 RPM) for males and 10–24 rad/s (95–229 RPM) for females when accelerating against resistance.

Using the flywheel's moment of inertia ($I = 6.25\ kg{\cdot}m^2$), the corresponding kinetic energy achievable through human effort can be estimated from Equation 1. At the upper range of reported angular velocities (28 rad/s), the stored energy is approximately 2.45 kJ; at more conservative sustained efforts (13 rad/s), the energy is approximately 0.53 kJ.

These angular velocities correspond to rotational speeds of 95–267 RPM, well within the safest resonance-free window (below 5,700 RPM). This confirms two important points:

1. Safety confirmation: Manual operation will remain safely within the lowest resonance-free window (<5,700 RPM), well below any critical speeds.
2. Capacity gap: The flywheel's full energy storage potential significantly exceeds what human power alone can deliver. The system is therefore under-utilized when powered solely by manual cranking.

The high-speed modal analysis thus serves its intended purpose: establishing absolute structural limits for safety validation, not operational targets. The exceptionally high critical speeds also provide a substantial safety margin should the flywheel ever be driven by other means (e.g., a small motor, solar-assist, or improved mechanical advantage systems) in future adaptations. This capacity gap points to opportunities for enhancing input methods, as discussed in Section 6.0.

3.4 Comparative Analysis with Alternative Storage and Pumping Technologies

To contextualise the proposed spring-assisted flywheel, Table 5 compares it with a conventional flywheel (no spring), lead-acid battery storage, and a diesel pump – the main alternatives for off-grid rural water pumping in Uganda.

Table 5: Comparative summary of storage and pumping options for rural off grid applications

Parameter	Proposed Spring-Assisted Flywheel	Conventional Flywheel (no spring)	Lead-Acid Battery	Diesel Pump
Energy efficiency	Higher than conventional	High	Low	Low
Additional energy storage	Elastic (springs, ~40 J)	None	Chemical (battery)	Chemical (fuel)
Consumables	None	None	Batteries every 2–4 years	Fuel, oil, filters
Maintenance	Low (bearings, belts)	Low (bearings)	High (terminals, electrolyte)	High (engine, fuel system)
Local repairability	High	High	Low	Moderate
Discharge duration	Minutes (extended by springs)	Seconds to minutes	Hours	Continuous (fuel-dependent)

The proposed spring-assisted flywheel offers higher energy efficiency than a conventional flywheel, while also adding elastic energy storage (~40 J) that extends discharge duration from seconds to minutes. Compared to lead-acid batteries, it avoids recurring replacement costs and local repairability challenges. Against diesel pumps, it eliminates fuel logistics and fuel emissions, at the cost of shorter continuous run time, an acceptable trade-off for community water needs where human-powered recharging is feasible several times per day.

3.5 Practical Deployment Considerations in Rural Uganda

While the design is technically sound, its real-world viability depends on local factors.

1. Local manufacturing feasibility: The flywheel, frame, and shaft can be fabricated in rural workshops using mild steel, basic lathe and welding equipment. Precision balancing and custom spring winding may require support from urban centres (e.g., Kampala, Mbarara).
2. Maintenance requirements: Bearings, belts, and springs are replaceable with basic hand tools. Training local artisans on spring fatigue monitoring and flywheel re-balancing would enhance long-term reliability.
3. Component durability: Steel components have an expected service life exceeding 20 years. The springs are designed for >1 million cycles (equivalent to >100 years of daily manual operation). The 3 mm mild steel guard with ISO 14120 compliance provides adequate fragment containment.

4. Cost accessibility: While the estimated material cost is likely to be prohibitive for an individual household, the system can be acquired collectively by a village, cooperative, or community group. Shared ownership, through village savings and loan associations (VSLAs), cooperative water user associations, or pay-as-you-pump schemes, distributes the financial burden and makes the technology affordable for rural communities.

These considerations confirm that the design is not only structurally robust but also practically deployable in the Ugandan context.

4.0 Findings

The finite element analysis results conclusively validate the structural integrity of the spring-assisted flywheel energy storage system. Several findings are particularly significant for the rural Uganda context:

1. Structural integrity confirmed

Static structural analysis demonstrated that all critical components operate well within material yield strengths. The shaft exhibited maximum principal stress of 0.294 MPa, representing merely 0.05% of its yield strength (530 MPa), while the frame showed maximum von Mises stress of 18.5 MPa, equivalent to 7.4% of its yield strength (250 MPa). These exceptionally low stress values confirm that both components operate entirely within the elastic regime with negligible risk of material failure.

2. Exceptional safety margins

Minimum factors of safety of 15 for the shaft and 13.5 for the frame substantially exceed the recommended minimum of 3.0 for rotating machinery [9]. This robustness is essential for a manually-operated system in a rural environment where operational conditions may vary and regular maintenance may be limited. The design can tolerate unexpected overloads, shock loads during manual cranking, and potential stress concentrations without risk of catastrophic failure, providing substantial reserve capacity for long-term reliability.

3. Minimal deformation ensures reliability

Shaft deformation of 1.1 micrometres and frame deformation of 0.78 mm guarantee that critical alignments between the flywheel, bearings, and belt drive system are maintained during operation. This preserves transmission efficiency, prevents premature component wear, and ensures consistent performance, important factors for long-term reliability in off-grid applications.

4. Critical speeds identified

Modal analysis established natural frequencies of 112.64 Hz, 112.69 Hz, 162.70 Hz, 293.21 Hz, and 293.22 Hz, corresponding to critical speeds of approximately 6,760 RPM, 9,762 RPM, and 17,593 RPM. These values represent absolute structural limits where resonant amplification of vibrations could occur.

5. Safe operating windows established

Modal analysis identified three resonance-free windows: below 5,700 RPM; 7,800–9,500 RPM; and 11,300–14,900 RPM. However, only the low-speed window (below 5,700 RPM) is recommended for sustained operation, as it completely avoids all mode shapes and provides maximum safety margin. The mid and high windows correspond to mode shapes with progressively larger deformation amplitudes (up to 0.1044 m) and should not be considered operational targets for the manually-powered system.

6. Design validated for local fabrication

The use of standard engineering materials (ASTM A36 mild steel, AISI 1045 medium carbon steel) readily available in Ugandan markets, combined with geometric dimensions achievable using standard workshop equipment, confirms that the design is not only technically sound but also practically realizable within local fabrication constraints. This contextual feasibility ensures that the system can be replicated, maintained, and sustained within rural Ugandan communities using locally available resources and workshop capabilities.

7. Human power capacity gap identified

Analysis of human arm cranking literature indicates that manual operation achieves only 95–267 RPM, utilizing less than 5% of the flywheel's rated speed capacity. While this confirms safe operation within resonance-free windows, it also reveals that the flywheel's full energy storage potential cannot be realized through human input alone.

5.0 Conclusion

This paper has presented the design and finite element validation of a spring-assisted flywheel energy storage system specifically tailored for groundwater pumping applications in rural Uganda. The design incorporates a 50 kg mild steel flywheel, double-torsion spring mechanism (18.5 Nm/rad stiffness), and 2:1 belt-pulley drive system, all selected for local availability and manufacturability.

Finite element analysis confirmed exceptional structural integrity, with minimum factors of safety of 15 for the shaft and 13.5 for the frame, substantially exceeding the recommended minimum of 3.0 for rotating machinery. This robustness ensures the system can withstand not only design loads but also unexpected dynamic forces realistic to community settings, while providing opportunities for future adaptations.

Modal analysis identified critical speeds at 6,760 RPM, 9,762 RPM, and 17,593 RPM, establishing three resonance-free operating windows. Based on human arm cranking literature [13], manual operation is expected to achieve only 95–267 RPM, well within the lowest and safest window (<5,700 RPM). The higher windows represent absolute structural limits, not operational targets, and are documented for completeness and future design adaptations.

The present study is limited to virtual validation; no physical prototype has been fabricated or tested. Therefore, the simulation-based findings must be confirmed through experimental work. A prototype will be fabricated following the specifications in Table 1 and the CAD model (Figure 1). Future experimental tests will measure energy retention (flywheel speed decay under zero load), discharge efficiency (mechanical input vs. electrical output), and spring contribution (comparative runtime with and without springs), as outlined in Recommendations 1–4. These experiments will provide the empirical evidence needed to fully validate the system's performance.

The validated design provides a technically sound foundation for prototype fabrication, offering a battery-free, mechanically robust alternative to diesel generators and solar-battery systems. This work contributes a context-appropriate solution aligned with Sustainable Development Goals for clean water and energy access, while supporting Uganda's national development priorities for rural transformation through appropriate technology.

6.0 Recommendations

Based on the findings of this study, the following recommendations are made:

1. Proceed to prototype fabrication

   The validated design should be translated into a physical prototype following the specifications in Table 1 and the CAD model developed in SolidWorks 2025.

2. Implement speed monitoring during testing

   During experimental evaluation, an optical encoder should be used to monitor rotational speed in real-time. The only recommended operating regime for sustained use is below 5,700 RPM. Based on human power literature [13], actual manual operation is expected to remain within 95–267 RPM, well inside this safest window. The higher windows (7,800–9,500 RPM and 11,300–14,900 RPM) are documented for completeness but should not be approached during manual testing due to the high deformation amplitudes of associated mode shapes.

3. Conduct experimental modal analysis

   Future work should include experimental modal testing to validate the analytical predictions and refine critical speed estimates.

4. Evaluate spring-assist contribution

   Performance testing should quantify the extension in operational runtime provided by the spring mechanism compared to non-spring configuration.

5. Explore optimization opportunities

   While current safety factors are exceptionally high, future iterations could explore material reduction or geometry optimization while maintaining adequate safety margins.

6. Explore enhanced input mechanisms

   Given that human cranking utilizes only a fraction of the flywheel's rated capacity, future work should investigate methods to increase input energy. Options include:

   i. Mechanical advantage systems (gearing, multi-speed drives)
   ii. Hybrid power sources (small solar-assisted motor drives)
   iii. Multi-user cranking stations
   iv. Improved ergonomic designs for sustained higher-power output

   Such enhancements could unlock more of the flywheel's storage potential while maintaining the battery-free, mechanically simple design philosophy.

Acknowledgements

The authors gratefully acknowledge the Department of Mechanical Engineering and the academic staff of the School of Engineering and Applied Sciences at Kampala International University for their valuable insights, constructive feedback, and professional guidance during the concept development and proposal stages of this research. Their positive critique, thoughtful recommendations, and scholarly engagement significantly strengthened the clarity, technical depth, and overall quality of this work.

References

UN-Water, "The United Nations World Water Development Report 2021: Valuing Water," United Nations, 2021.

UBOS, "Uganda National Household Survey 2019/2020," Uganda Bureau of Statistics, Kampala, 2020.

World Bank, "Beyond connections: Energy access redefined," World Bank Group, Washington, DC, 2018.

K. C. Divya and J. Østergaard, "Battery energy storage technology for power systems—An overview," *Electric Power Systems Research*, vol. 79, no. 4, pp. 511-520, 2009.

A. G. Olabi, T. Wilberforce, M. A. Abdelkareem, and M. Ramadan, "Critical review of flywheel energy storage system," *Energies*, vol. 14, no. 8, p. 2159, 2021.

R. Okou, A. B. Sebitosi, and M. A. Khan, "The potential impact of small-scale flywheel energy storage technology on Uganda's energy sector," *Renewable Energy*, vol. 34, no. 11, pp. 2433-2438, 2009.

MWE, "Water and environment sector performance report," Ministry of Water and Environment, Uganda, Kampala, 2020.

World Bank, "Solar pumping for rural water supply: Life-cycle costs from eight countries," The World Bank, Washington, DC, 2018.

A. K. Arani, H. Karami, G. B. Gharehpetian, and M. S. A. Hejazi, "Review of flywheel energy storage systems structures and applications in power systems," *Renewable and Sustainable Energy Reviews*, vol. 69, pp. 9-18, 2017.

R. G. Budynas and J. K. Nisbett, *Shigley's Mechanical Engineering Design*, 10th ed. McGraw-Hill, 2015.

F. Meng, H. Zhang, F. Yang, and M. Niu, "An energy-saving pumping system with novel springs energy storage devices: Design, modeling, and experiment," *Energy*, vol. 141, pp. 1284-1293, 2017.

ISO 14120:2015, "Safety of machinery — Guards — General requirements for the design and construction of fixed and movable guards," International Organization for Standardization, 2015.

M. Vanderthommen, M. Francaux, D. Johnson, M. Dewan, Y. Lewyckyj, and X. Sturbois, "Measurement of the power output during the acceleration phase of all-out arm cranking exercise," *International Journal of Sports Medicine*, vol. 18, no. 8, pp. 600-606, Nov. 1997.